SIAM REVIEW
Vol. 43, No. 3, pp. 478–495

The Lindstedt–Poincaré Technique as an Algorithm for Computing Periodic Orbits*

Divakar Viswanath†

Abstract. The Lindstedt–Poincaré technique in perturbation theory is used to calculate periodic orbits of perturbed differential equations. It uses a nearby periodic orbit of the unperturbed differential equation as the first approximation. We derive a numerical algorithm based upon this technique for computing periodic orbits of dynamical systems. The algorithm, unlike the Lindstedt–Poincaré technique, does not require the dynamical system to be a small perturbation of a solvable differential equation. This makes it more broadly applicable. The algorithm is quadratically convergent. It works with equal facility, as examples show, irrespective of whether the periodic orbit is attracting, or repelling, or a saddle. One of the examples presents what is possibly the most accurate computation of Hill's orbit of lunation since its justly celebrated discovery in 1878.

Key words. periodic orbits, Linstedt–Poincaré technique

AMS subject classifications. 65L10, 65L20, 37C27

PII. S0036144500375292

1. Introduction.

Periodic orbits are everywhere in the study of differential equations. Keplerian motion under an inverse square law force is elliptic and periodic, and the solution of the three-body problem that forms the foundation of the Hill–Brown theory in celestial mechanics is also periodic [20]. Every area of science has its own oscillatory phenomena and these are usually periodic solutions of differential equations. The focus of this paper is a fast and accurate algorithm for computing periodic orbits.

The solution $x(t)$ of the ordinary differential equation $\dot{x}(t) = f(x)$, $x \in R^d$, is a periodic orbit if $x(t+T) = x(t)$ for all real t. The number T is its period. The unrestrictive assumption of twice continuous differentiability of $f(x)$ suffices here and in section 3. Usually $f(x)$ is analytic. Periodicity of the orbit simplifies its stability analysis, and it is generally sufficient to look at the linearization [12]. In the linearization $\dot{y}(t) = A(t)y$, $A(t) = \frac{\partial f(x)}{\partial x}|_{x=x(t)}$, $A(t)$ is also periodic with period T. Let $Y(t)$, where $Y(0)$ is the $n \times n$ identity matrix, be the fundamental solution of this linear equation. All the n columns of $Y(t)$ solve $\dot{y}(t) = A(t)y$. The matrix $Y(T)$ is the monodromy of the periodic orbit.

The eigenvalues of the monodromy are invariant under a change of variables. There is always an eigenvalue equal to 1 corresponding to perturbations along the

*Received by the editors July 19, 2000; accepted for publication (in revised form) January 24, 2001; published electronically August 1, 2001.
http://www.siam.org/journals/sirev/43-3/37529.html

†Departments of Computer Science and Mathematics, University of Chicago, 1100 E. 58th St., Chicago, IL 60637 (divakar@cs.uchicago.edu).

orbit. The eigenvalues excluding 1 are called characteristic multipliers. If all the characteristic multipliers are less than 1 in magnitude, the orbit will attract an open neighborhood and is called attracting. If all are greater than 1 in magnitude, the orbit will repel an open neighborhood and is called repelling. If some are greater and some are less than 1, the orbit is a saddle. There is the additional possibility that some of the characteristic multipliers might actually lie on the unit circle. Characteristic multipliers and stability of periodic orbits are clearly discussed by Hale [12] and by Robinson [19].

The monodromy and the characteristic multipliers determine to a large extent the effectiveness of every algorithm for computing periodic orbits. A natural approach for computing a periodic orbit is to pick a point close to the periodic orbit and follow the trajectory from that point using an ODE solver. The trajectory will converge if the periodic orbit is attracting. Following the trajectory backward in time will converge if the periodic orbit is repelling. When the periodic orbit is a saddle, however, this approach has no chance of success at all. Another issue is that following trajectories, when the periodic orbit converges at all, it converges only linearly. Even if the trajectory is followed exactly, the distance to the periodic orbit will decrease approximately by a constant factor in one period. Thus, for example, if the distance to the periodic orbit is 0.1 to begin with and the leading characteristic multiplier within the unit circle has magnitude 0.8, the distance of the trajectory from the periodic orbit could be 0.08, .064, .0512, etc., after successive periods. However, the tools for following trajectories, ranging from Runge–Kutta solvers to multistep methods, are numerous and very well developed, and it is worthwhile trying to use them. The third example in section 4 uses a slight modification of this natural approach to get quadratic convergence. Thus if this modification is used, the distance to the periodic orbit after successive periods can decrease like 0.1, .01, .0001, .00000001,.... The advantage of quadratic convergence over linear convergence is readily apparent.

The computer package AUTO written by Doedel and others [6] has been used for finding periodic orbits. AUTO's extensive capabilities include finding periodic orbits, solving boundary value problems, computing local and global bifurcations, and computing homoclinic orbits. It is also well documented. AUTO uses piecewise polynomials and collocation at Gauss–Legendre points to compute periodic orbits. The algorithm is superconvergent at mesh points.

Like AUTO, the algorithms proposed by Choe and Guckenheimer [1] and Guckenheimer and Meloon [10] treat the problem of finding a periodic orbit as a sort of boundary value problem. The algorithms use automatic differentiation [8] to tightly control the accuracy of the approximation to the periodic orbit. What follows is a description of one of their algorithms. Assume that the desired periodic orbit of $\dot{x}(t) = f(x)$ is at the points $x_1, x_2, \ldots, x_{N-1}$ at times $t_1 < t_2 < \cdots < t_{N-1}$ and that it returns to x_1 for the first time at $t = t_N$. Thus $t_N - t_1$ is its period. We won't know the points x_i and t_i initially, of course, but the algorithm assumes reasonable approximations to begin with. Denote the time t map induced by the flow by $\phi_t : R^d \to R^d$. Then for the periodic orbit,

$$\begin{aligned} \phi_{t_2 - t_1}(x_1) &= x_2 \\ &\vdots \\ \phi_{t_N - t_{N-1}}(x_{N-1}) &= x_1. \end{aligned}$$

Guckenheimer and Meloon [8] treated this as a set of nonlinear equations to be solved

for t_i and x_i beginning with a reasonable approximation. Some additional constraints, which are mostly intuitive, need to be imposed. They use automatic differentiation in two ways. The first use is as an accurate ODE solver for computing the maps $\phi_{t_{i+1}-t_i}$. The second use is to obtain the Jacobians of the maps, which are needed to apply Newton's method. There are other variants of this forward multiple shooting algorithm: one is a symmetric multiple shooting algorithm and another is based on Hermite interpolation.

Before making further comments, we establish an analogy. The problem of finding periodic orbits is certainly harder than the problem of finding fixed points of a given flow. The problem of finding fixed points, on the other hand, is exactly the same as the extensively investigated problem of solving the system of nonlinear equations $f(x) = 0$. It is widely believed that this last problem is unsolvable in general without a sufficiently good starting approximation. See, for example, the comments about global optimization in [3]. Therefore, the necessity of good approximations to x_i and t_i must not be considered a limitation of the Guckenheimer–Meloon algorithm. A good starting approximation is an inevitable requirement of any algorithm for computing periodic orbits. The monodromy matrix of the periodic orbit plays the same role as the Jacobian of $f(x)$ at the fixed point or zero.

Wisely, Guckenheimer and Meloon [8] emphasized accuracy over speed. The algorithm derived in section 2 is quadratically convergent. Section 3 gives a proof of quadratic convergence. Examples in section 4 demonstrate that the convergence in practice is quadratic and very smooth. The analogy with zero finding for nonlinear systems makes it clear that quadratic convergence is as good as can be expected. Guckenheimer and Meloon included a proof of convergence but did not discuss the rate of convergence. Doedel proved convergence of a collocation method in [4].

The algorithm for computing periodic orbits in section 2 is a polyphony of three themes: the Lindstedt–Poincaré technique from perturbation theory, Newton's method for solving nonlinear systems, and Fourier interpolation. The basis of Newton's method is the linearization of the nonlinear system of equations. In section 2, we linearize the differential equation around an approximate periodic orbit. The author [24] has used a similar approach to analyze the accumulation of global errors while solving initial value problems using Runge–Kutta-type methods. Indeed, the proof of the convergence theorem in section 3 is quite similar to the proof of Theorem 2.1 in [24]. Fourier interpolation is a natural choice for periodic orbits, but as the third example in section 4 shows, of the three themes, this is the most dispensable.

The Duffing oscillator has emerged as the favorite starting point for introducing the Lindstedt–Poincaré technique. Section 2 follows this tradition. The concluding section 5 comments on computing bifurcations.

Lau, Cheung and Wu [15] and Ling and Wu [16] independently proposed harmonic balance methods for computing periodic orbits. Their methods use Fourier series as ours do. The main part of the computation in harmonic balance methods is the solution of a linear system of dimension nd, where the differential equation is d-dimensional and the Fourier series are of width n. The linear systems are dense because of the global nature of Fourier interpolation, and the $O(n^3)$ cost of solving those systems becomes prohibitive for large n. Computation of periodic orbits with accuracy comparable to machine precision has not been demonstrated using harmonic balance methods as far as we know. In a proper implementation [25], the cost of our algorithm depends on n like $O(n \log n)$.

For computing periodic orbits and bifurcations, AUTO [6] has proved itself over nearly two decades of use. Doedel [5] surveys the large body of work that has gone into

this package. AUTO's algorithm and the Guckenheimer–Meloon algorithms [10] are adaptive. Since the linear systems that they form are sparse, the cost of solution is only linear in the number of mesh points in one case and in the number of shooting points in the other. Their adaptivity makes them superior choices for computing periodic orbits that combine slow and rapid variation in different regions. When a periodic orbit is analytic, its Fourier coefficients decrease exponentially fast, making its Fourier representation compact. For such periodic orbits, our algorithm will be advantageous. Another feature of our algorithm is the ease with which global constraints on the periodic orbit can be enforced as shown by the coupled Josephson junctions example in section 4.

2. An Algorithm for Computing Periodic Orbits. The Duffing oscillator governed by $\ddot{q} = -q - \epsilon q^3$ is a small perturbation of the linear oscillator. With $p = \dot{q}$, its Hamiltonian is $p^2/2 + q^2/2 + \epsilon q^4/4$. In $q - p$ phase space, the flow is along the level curves of this Hamiltonian. Therefore, every trajectory of the Duffing equation is a periodic orbit. However, not all periodic orbits of the Duffing equation have the same frequency or period.

We seek a solution to the Duffing equation with $q(0) = 1$, $p(0) = 0$. The unperturbed equation with $\epsilon = 0$ has the solution $q(t) = \cos(t)$, $p(t) = -\sin(t)$. The Lindstedt–Poincaré technique recognizes that the actual orbit will have a period slightly different from 2π. In the equations

$$\begin{aligned} \tau &= \omega t, \\ \omega \frac{dq}{d\tau} &= p, \\ \omega \frac{dp}{d\tau} &= -q - \epsilon q^3, \end{aligned} \tag{2.1}$$

ω allows for a rescaling of time. The Lindstedt–Poincaré technique tries to find a solution for q and p that is 2π periodic in τ and a value of ω close to 1 to account for the slight difference of the period from 2π. The starting guess is $\omega_0 = 1$, $q_0(\tau) = \cos(\tau)$, and $p_0 = -\sin(\tau)$.

This guess doesn't solve (2.1). So try to correct it to $\omega_1 = \omega_0 + \delta\omega$, $q_1(\tau) = q_0(\tau) + \delta q(\tau)$, and $p_1(\tau) = p_0(\tau) + \delta p(\tau)$. The corrections δq and δp must also be 2π periodic functions of τ. Substitute into (2.1) to get

$$\begin{aligned} (\omega_0 + \delta\omega)\frac{d\delta q}{d\tau} &= \delta p + \left(p_0 - (\omega_0 + \delta\omega)\frac{dq_0}{d\tau} \right) \\ &= \delta p + \delta\omega \sin\tau, \\ (\omega_0 + \delta\omega)\frac{d\delta p}{d\tau} &= -(q_0 + \delta q) - \epsilon(q_0 + \delta q)^3 - (\omega_0 + \delta\omega)\frac{dp_0}{d\tau} \\ &= (-1 - 3\epsilon\cos^2\tau)\delta q - \epsilon\cos^3\tau + \delta\omega\cos\tau + (\delta q)^2(\cdots) + (\delta q)^3(\cdots). \end{aligned}$$

Linearize and neglect all terms of order δ^2 and higher to get

$$\omega_0 \frac{d}{d\tau}\begin{pmatrix}\delta q \\ \delta p\end{pmatrix} = \begin{pmatrix} 0 & 1 \\ -1 - 3\epsilon\cos^2\tau & 0 \end{pmatrix}\begin{pmatrix}\delta q \\ \delta p\end{pmatrix} + \delta\omega\begin{pmatrix}\sin\tau \\ \cos\tau\end{pmatrix} - \begin{pmatrix} 0 \\ \epsilon\cos^3\tau \end{pmatrix}. \tag{2.2}$$

Equation (2.2) will be solved for δq, δp, and $\delta\omega$ in the following way. The initial conditions require $q(0) = 1$ and $p(0) = 0$. Since q_0 and p_0 already obey this requirement,

Table I *The exact ω for the periodic orbit of the Duffing equation $\ddot{q} = -q - \epsilon q^3$, $q(0) = 1$, $\dot{q}(0) = 0$, is $1.0367169070746336487563360 95\ldots$ for $\epsilon = 0.1$. The starting approximation is $q = \cos(t)$, $p = \dot{q} = -\sin(t)$. The iterations use 32-point Fourier series to represent q and p. The convergence to the exact solution is clearly quadratic.*

Iteration	ω	Residual error	Energy error
0	1.00000000000000	1e-1	2.5e-2
1	1.03726228918977	2.3e-3	1.7e-4
2	1.03671693072840	9.2e-7	3.8e-7
3	1.03671690707462	4.4e-14	2.8e-14
4	1.03671690707463	1.1e-15	1.0e-15
5	1.03671690707463	5.4e-16	3.3e-16

set $\delta q(0) = 0$ and $\delta p(0) = 0$. The solution of (2.2) then takes the form

$$\begin{pmatrix} \delta q \\ \delta p \end{pmatrix} = f_1(\tau) + \delta\,\omega f_2(\tau).$$

The R^2-valued functions f_1 and f_2 can be computed by applying an accurate ODE solver to (2.2). Choose $\delta\omega$ to minimize the 2-norm of $f_1(2\pi) + \delta\omega f_2(2\pi)$. This makes the corrections δq and δp as close to being 2π periodic in τ as possible. After these corrections are added to the initial guess, ω_1, q_1, p_1 will be closer to an exact solution of the Duffing equation.

The passage from ω_0, q_0, p_0 to ω_1, q_1, p_1 follows the Lindstedt–Poincaré technique, but the presentation is different from the standard accounts in Kevorkian and Cole [14] and Nayfeh [18]. There is also a difference that goes beyond presentation. To make the calculations analytically feasible, the usual applications of this technique ignore the ϵ term in $-1 - 3\epsilon\cos^2\tau$. Ignoring that term gives $\omega_1 = 1 + 3\epsilon/8$. For $\epsilon = 0.1$, $1 + 3\epsilon/8 = 1.0375$ is worse than the approximation obtained after one iteration in Table 1. An early use of the Lindstedt–Poincaré technique was to get rid of the secular terms in planetary theories that used Lagrange's orbital elements. It is also sometimes called the method of strained coordinates.

Table 1 shows the effect of successive iterations. The energy error is the maximum deviation from the Hamiltonian along the approximate periodic orbit computed by the iteration. The residual error is the maximum of $|\omega_i\dot{q}_i(\tau) - p_i|$ and $|\omega_i\dot{p}_i(\tau) + q_i + \epsilon q_i^3|$ along the orbit. The magnitude of the Fourier coefficients of $q(\tau)$ are shown in Figure 1. The use of Fourier series in the algorithm is yet to be explained.

For a continuous 2π periodic function $x(\tau)$, the Fourier series takes the form $\sum_{k=-\infty}^{\infty} a_k \exp(ik\tau)$. The rate of decrease of $|a_k|$ as $|k| \to \infty$ depends upon the smoothness of $x(\tau)$. In particular, when $x(\tau)$ is analytic in a strip about the real line, the decrease is exponential. A Fourier series of width $2p+1$ picks up the $2p+1$ coefficients from a_{-p} to a_0 to a_p. A Fourier series of width $2p$ uses $2p$ coefficients, but one of the coefficients is taken to be a coefficient of $\cos(pt)$. To compute n Fourier coefficients of $x(\tau)$, the fast Fourier transform (FFT) is applied to the function evaluated at n equispaced points in $[0, 2\pi)$. The width n of the Fourier series must be sufficiently large to pick up all the coefficients above a threshold comparable to the machine precision. The kth coefficient of the derivative $\dot{x}(\tau)$ is ika_k, except when k is the index of the cos term in a Fourier series of even width. If $x_1, \ldots, x_m$ are 2π periodic, so is $f(x_1, \ldots, x_m)$. To obtain its Fourier series from those of the x_i, interpolate x_i at equispaced points in $0 \le \tau < 2\pi$, evaluate f at those points, and apply the FFT. The inverse FFT can be used to interpolate a Fourier series at

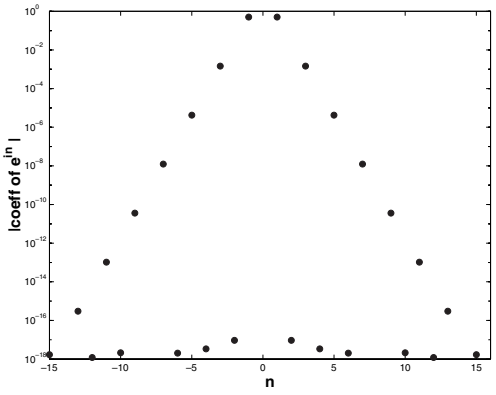

Fig. I *The magnitudes of the Fourier coefficients of q of the periodic orbit of the Duffing equation $\ddot{q} = -q - \epsilon q^3$, $q(0) = 1$, $\dot{q}(0) = 0$, with $\epsilon = 0.1$. The coefficients that cling to the bottom of the plot are all rounding errors. Clearly, 32 points is nearly the minimum width of a Fourier series that can pick up all the frequencies with amplitudes above $1e-16$, the IEEE machine precision. The errors near $n = 0$ are due to aliasing.*

equispaced points. Trefethen [23] gave a lucid account of matters related to the use of Fourier series. We comment about aliasing errors at the beginning of section 4.

The algorithm below applies to isolated orbits. When the orbit to be approximated is not isolated, as for the Duffing equation above, the modifications needed are minor. They are given at the end. The problem is to find an isolated orbit of the dynamical system $\dot{x}(t) = f(x)$, $x \in R^d$. Rescale time as before using $\tau = \omega t$ and ask for a frequency ω and a 2π periodic orbit of the dynamical system $\omega\dot{x}(\tau) = f(x)$. The starting guesses ω_0 for the frequency and $x_0(\tau)$ for the periodic orbit must be sufficiently close to the periodic orbit. However, $x_0(0)$ need not be on the orbit as it was for the Duffing equation. The first guess $x_0(\tau)$ must be 2π periodic. Assume it is given as d Fourier series, one for each coordinate in R^d. The iteration to generate improved approximations ω_1 and $x_1(\tau)$ is made up of the following steps:

1. Compute the Fourier series for all d^2 entries of $A(\tau)$, which is defined as $A(\tau) = \frac{\partial f(x)}{\partial x}\big|_{x=x_0(\tau)}$.
2. Compute d Fourier series for the residual $r(\tau) = f(x_0(\tau)) - \omega_0\dot{x}_0(\tau)$.
3. Compute d Fourier series for the derivative $\dot{x}_0(\tau)$.
4. Set up the *correction equation*

$$\omega_0\dot{y}(\tau) = A(\tau)y + r(\tau) - \delta\omega\dot{x}_0(\tau). \tag{2.3}$$

   This correction equation can be matched with (2.2) term by term. It can be derived in an almost identical manner. Take the fundamental solution of $\omega_0\dot{y}(\tau) = A(\tau)y$ to be $Y(\tau)$, with $Y(0)$ the identity matrix and $M = Y(2\pi)$ so that M is the approximate monodromy for the periodic orbit. The general solution of (2.3) written as

$$y(\tau) = Y(\tau)y(0) + f_1(\tau) - \delta\omega f_2(\tau) \tag{2.4}$$

   allows the choice of $y(0)$. Use an accurate ODE solver to compute the fundamental solution $Y(\tau)$ and $f_1(\tau)$ and $f_2(\tau)$.
5. $\delta\omega$ and $y(0)$ will be chosen to make $y(\tau)$ 2π periodic. Kevorkian and Cole [14] showed an application of the Lindstedt–Poincaré technique that involves

adjusting the initial condition. Clearly, $y(2\pi) = My(0) + f_1(2\pi) - \delta\omega f_2(2\pi)$. Requiring $y(2\pi) = y(0)$ gives d linear equations for the $d+1$ real unknowns $y(0)$ and $\delta\omega$. But varying $x(0)$ along the periodic orbit gives different representations of the same periodic orbit. Therefore, impose the additional requirement that $y(0)$ must be orthogonal to the vector field at $x_0(0)$. Solve the linear system

$$\begin{pmatrix} I - M & f_2(2\pi) \\ f(x_0(0))^T & 0 \end{pmatrix} \begin{pmatrix} y(0) \\ \delta\omega \end{pmatrix} = \begin{pmatrix} f_1(2\pi) \\ 0 \end{pmatrix},$$

where I is the identity in $R^{d,d}$, to obtain $y(0)$ and $\delta\omega$.

6. Obtain d Fourier series for $y(\tau)$ by interpolating $Y(\tau)y(0)$, $f_1(\tau)$, and $f_2(\tau)$ in equispaced intervals in $[0, 2\pi)$.
7. The new approximations are $x_1(\tau) = x_0(\tau) + y(\tau)$ and $\omega_1 = \omega_0 + \delta\omega$.

The iteration can be continued to obtain $\omega_2, x_2(\tau)$ from $\omega_1, x_1(\tau)$ and so on. Propagating the residual error $r(\tau)$ using the linearization of the differential equation $\omega\dot{x}(\tau) = f(x)$ along the approximate orbit leads to $f_1(\tau)$. Propagating $\dot{x}_0(\tau)$ along the approximate orbit leads to $f_2(\tau)$. Therefore, $f_2(\tau)$ will be roughly parallel to the vector field along the approximate orbit. The correction equation (2.3) tries to cancel out the residual error. From the interpretation we have given to f_1 and f_2, it follows that the $\delta\omega$ term in (2.4) will mainly cancel out the component of the residual error along the orbit, while the $y(0)$ term will mainly cancel out the error transverse to the orbit.

If it is known that $x_0(0)$ is on the periodic orbit, we can take $y(0) = 0$ and $\delta\omega = \frac{f_2(2\pi)^T f_1(2\pi)}{f_2(2\pi)^T f_2(2\pi)}$. Table 1 and Figure 1 use an implementation of the iteration with this modification.

Each iteration of the algorithm spends almost all its time in the ODE solver used in step 4 for computing $Y(\tau)$, $f_1(\tau)$, and $f_2(\tau)$. The Duffing equation and the examples in section 4 used MATLAB's `ode45` with the option `odeset('AbsTol',1e-8, 'RelTol', 1e-8)`. The MATLAB code for implementing the iteration for the Duffing equation and for the examples in section 4 was about 75 lines.

3. Proof of Quadratic Convergence. The proof of quadratic convergence (in Theorem 3.1 below) of the algorithm in the preceding section is similar to the proof of Theorem 2.1 in [24] in its use of the linear variation of constants formula. Hale [12] gave a fine description of the linear variation of constants formula, as of many other topics. Unlike the proof of quadratic convergence of Newton's method in Dennis and Schnabel [3], the proof below uses second derivative information. Quadratic convergence fails when 1 is a multiple eigenvalue of the monodromy. When 1 is a multiple eigenvalue, the constant σ_2 in Theorem 3.1 becomes zero at the periodic orbit. This failure is similar to the loss of quadratic convergence in Newton's method when the Jacobian at the root is singular.

The proof ignores all errors made by the ODE solvers in step 4 of the algorithm. In other words, the linear ODEs in step 4 are assumed to be solved exactly. Both Theorem 3.1 and its proof use notation introduced in section 2. The vector norm in this section is length in Euclidean space. The matrix norm is the induced matrix norm.

THEOREM 3.1. *Assume that $\bar{\omega}$ and $\bar{x}(\tau)$ give a hyperbolic 2π periodic orbit of $\omega\dot{x}(\tau) = f(x)$. As explained in section 2, they also give a $2\pi/\bar{\omega}$ periodic orbit of $\dot{x}(t) = f(x)$. Assume that $x \in R^d$ and that $f(x)$ is twice continuously differentiable.*

Let ω_0 and $x_0(\tau)$, which must be 2π periodic, be approximations to $\bar{\omega}$ and $\bar{x}(\tau)$. Let $\delta\bar{\omega} = \bar{\omega} - \omega_0$ and $\bar{y} = \bar{x} - x_0$. Assume

$$\begin{aligned} |\delta\bar{\omega}| &< \epsilon, \\ \|\bar{y}(\tau)\| &< \epsilon, \quad 0 \le \tau \le 2\pi, \\ \|\dot{\bar{y}}(\tau)\| &< \epsilon, \quad 0 \le \tau \le 2\pi. \end{aligned}$$

Let ω_1 and x_1 be the new approximations generated by the iteration in section 2. Then

$$\begin{aligned} |\omega_1 - \bar{\omega}| &< C_1\epsilon^2, \\ \|x_1(\tau) - \bar{x}(\tau)\| &< C_2\epsilon^2, \quad 0 \le \tau \le 2\pi, \\ \|\dot{x}_1(\tau) - \dot{\bar{x}}(\tau)\| &< C_3\epsilon^2, \quad 0 \le \tau \le 2\pi \end{aligned}$$

for $\epsilon < \epsilon_0$ for some $\epsilon_0 > 0$. The constants C_1, C_2, and C_3 are given by $C_1 = c_1\sigma_1/\sigma_2$, $C_2 = c_2(\sigma_1/\sigma_2 + \sigma_1)$, and $C_3 = c_2(\sigma_1/\sigma_2 + \sigma_1)$. The constants c_1, c_2, and c_3 depend only upon the second derivative of $f(x)$ in a neighborhood of the periodic orbit. The constants σ_1 and σ_2 are given by

$$\begin{aligned} \sigma_1 &= \sup_{0 \le s \le t \le 2\pi} \|Y(t)Y^{-1}(s)\|, \\ \sigma_2 &= \sigma_{min}\left(\begin{pmatrix} I - M & f_2(2\pi) \\ f(x_0(0))^T & 0 \end{pmatrix}\right). \end{aligned}$$

The definitions of $Y(t)$ and M are given in section 2 and σ_{min} is the minimum singular value of the matrix.

Proof. The assumption about $\bar{\omega}$, $\bar{x}$ and the definitions of $\delta\bar{\omega}$ and $\bar{y}$ imply

$$(\omega_0 + \delta\bar{\omega})\frac{d(x_0 + \bar{y})}{d\tau} = f(x_0 + \bar{y}),$$

which is the same as

$$\omega_0\frac{d\bar{y}}{d\tau} = \frac{\partial f}{\partial x}\Big|_{x=x_0(\tau)}\bar{y} + (f(x_0(\tau)) - \omega_0\dot{x}_0(\tau)) - \delta\bar{\omega}\dot{x}_0(\tau) + (\text{remainder}(x(\tau), \bar{y}(\tau)) - \delta\bar{\omega}\dot{\bar{y}}).$$

The remainder term above is obtained by Taylor-expanding $f(x_0 + \bar{y})$ about x_0. The remainder is necessarily 2π periodic. The above equation can be written as

$$\omega_0\frac{d\bar{y}}{d\tau} = \frac{\partial f}{\partial x}\Big|_{x=x_0(\tau)}\bar{y} + (f(x_0(\tau)) - \omega_0\dot{x}_0(\tau)) - \delta\bar{\omega}\dot{x}_0(\tau) + p(\tau), \tag{3.1}$$

where $p(\tau)$ is 2π periodic. The upper bounds on $\bar{y}$ and $\delta\bar{\omega}$ and the differentiability assumption on f imply that $\|p(\tau)\| < c\epsilon^2$ for a constant c which depends only upon the second derivative of f in a neighborhood of the periodic orbit. Think of (3.1) as a linear differential equation to be solved for $\bar{y}$. Then the general solution can be written as

$$\bar{y}(\tau) = Y(\tau)\bar{y}(0) + f_1(\tau) - \delta\bar{\omega}f_2(\tau) + P(\tau). \tag{3.2}$$

Here $Y(\tau)$, $f_1(\tau)$, and $f_2(\tau)$ are as defined in section 2, while $P(\tau)$ is given by the linear variation of constants formula

$$P(\tau) = \int_{s=0}^{\tau} Y(\tau)Y^{-1}(s)p(s)ds. \tag{3.3}$$

Similar integral expressions can be written down for f_1 and f_2, but that won't be necessary.

All the error after the first iteration arises because the iteration uses the general solution (2.4), which is

$$y(\tau) = Y(\tau)y(0) + f_1(\tau) - \delta\omega f_2(\tau),$$

instead of (3.2). Thus the term $P(\tau)$, which can be bounded as $\|P\| < c'\sigma_1\epsilon^2$, is what is missing. This term picks up all the error caused by the linearization.

The rest of the proof is routine. We show the proof only for the bound on $\omega_1 - \bar{\omega}$. If the iteration were to use (3.2), the linear equation for determining $\bar{y}(0)$ and $\delta\bar{\omega}$ would be

$$\begin{pmatrix} I - M & f_2(2\pi) \\ f(x_0(0))^T & 0 \end{pmatrix} \begin{pmatrix} \bar{y}(0) \\ \delta\bar{\omega} \end{pmatrix} = \begin{pmatrix} f_1(2\pi) \\ 0 \end{pmatrix} + \begin{pmatrix} P(2\pi) \\ 0 \end{pmatrix}.$$

However, the actual iteration neglects the $P(2\pi)$ term. Therefore, the errors $\|y(0) - \bar{y}(0)\|$ and $|\delta\omega - \delta\bar{\omega}|$ can be bounded above by $c\sigma_1\epsilon^2/\sigma_2$ for a suitable constant c. □

4. Examples. The first three examples in this section are drawn from Guckenheimer and Meloon [10]. The fourth example is based on Hill's famous work on the motion of the moon. In every case, the quadratic convergence of the algorithm in section 2 is clearly demonstrated. The first three examples include brief comparisons of our computations with those in [10].

The computations give all the 15 digits of precision possible in IEEE arithmetic of the frequencies or periods of the periodic orbits in all the examples. Characteristic multipliers are determined with equal precision in all examples but the last.

The implementation of the algorithm must pay attention to the possibility of aliasing. The system

$$\begin{aligned} \dot{x} &= -y + \mu x(1 - \sqrt{x^2 + y^2}), \\ \dot{y} &= x + \mu y(1 - \sqrt{x^2 + y^2}) \end{aligned}$$

has a limit cycle along the circle $x^2 + y^2 = 1$ for $\mu \neq 0$. The limit cycle is attracting for positive μ. Let the starting guesses be $x = \cos t + \epsilon \cos mt$ and $y = \sin t$. Evaluate the vector field along this approximate curve to $O(\epsilon)$ to get

$$\begin{pmatrix} -\sin t + \varepsilon\mu(\frac{\cos mt}{2} - \frac{\cos(m-2)t}{4} + \frac{\cos(m+2)t}{4}) \\ \cos\, t + \varepsilon\mu(\frac{\cos mt}{\mu} - \frac{\sin(m-2)t}{4} + \frac{\sin(m+2)t}{4}) \end{pmatrix}.$$

If the Fourier series is wide enough to pick up $\sin mt$ and $\cos mt$ terms but not wide enough to pick up $\sin(m+2)t$ and $\cos(m+2)t$ terms, the latter two frequencies can't be represented and are aliased to some lower frequencies. The correction equation has no chance of removing this $O(\epsilon)$ error. Thus, once there is error in some of the higher frequencies, it will persist throughout the computation. Therefore, the Fourier series may have to be wider than the minimum width needed to represent the periodic orbit, and very crucially for the success of the algorithm, the starting guess must not have high frequency errors. It is best to entirely remove about half or two-thirds of all the frequencies at the higher end from the starting guess.

At the end of every iteration, the Fourier series representing $x(\tau)$ must be forced into representing purely real functions. The use of the FFT creates a complex part because of rounding errors, and upon repeated iterations, this complex part may excite an instability.

Table 2 *The accurate digits in ω are underlined. The top eigenvalue of the monodromy is* 1 *for the exact orbit. However, M is only an approximation to the exact monodromy. The characteristic multiplier, which is the other eigenvalue of the monodromy, is* 0.03815204168599.

Iteration	ω	Energy error	Top eigenvalue of M
0	0.81178104743922	4.4e-3	1.01798286617795
1	0.81525369936630	1.3e-04	0.99953566116580
2	0.81519336337922	1.2e-07	0.99999930843800
3	0.81519335086431	3.1e-14	0.99999999999723
4	0.81519335086431	5.0e-16	0.99999999999752

4.1. Periodic Orbit along the Curve $x^2 - y^2 + 2y^3/3 + .07 = 0$. The system

$$\dot{x} = y - y^2 - x(x^2 - y^2 + 2y^3/3 + 0.07),$$
$$\dot{y} = x + (y - y^2)(x^2 - y^2 + 2y^3/3 + 0.07)$$

has an attracting limit cycle along the curve $x^2 - y^2 + 2y^3/3 + .07 = 0$. Table 2 summarizes a computation that used a Fourier series of width 64. The energy error in that table is the maximum of $|x^2 - y^2 + 2y^3/3 + .07|$ for $0 \le \tau < 2\pi$. Our computation easily matches the accuracy in [10].

4.2. Coupled Josephson Junctions. An uncoupled Josephson junction is described by $\beta\ddot{\phi}+\dot{\phi}+\sin\phi = I$. This equation also describes a forced, damped pendulum. The parameter β is named after Stewart and McCumber. Denote the unique periodic orbit by $\phi = h(t)$. Over one period, $h(t)$ increases by 2π, but $\dot{h}(t)$ is exactly periodic. Thus the pendulum goes over in every period. The equation for N coupled Josephson junctions is

$$\beta\ddot{\phi}_j + \dot{\phi}_j + \sin\phi_j + \dot{Q} = I, \qquad j = 1, \ldots, N,$$
$$L\ddot{Q} + R\dot{Q} + \frac{Q}{C} = \frac{1}{N}(\dot{\phi}_1 + \cdots + \dot{\phi}_N).$$

Watanabe and Swift [26] show an electrical circuit in which the parameters I, L, R, and C are the bias current, the inductance, the resistance, and the capacitance, respectively. They seek solutions of the coupled equations that take the form $\phi_1 = g(t)$, $\phi_2 = g(t+T/N)$, and so on until $\phi_N = g(t+(N-1)T/N)$, where $g(t)$ increases by 2π over the period T. Their interest is in particular in the stability of such *splay-phase* solutions. They say that various uses have been proposed for splay-phase solutions of coupled Josephson junctions, including use as computer memory, and presumably the practicality of these proposals could depend upon the stability of splay-phase solutions. In a splay-phase solution of period T, the period of Q will be $T/4$.

Table 3 shows computations of two splay-phase solutions. Both computations use $I = 2.5$, $L = 0.75$, $R = 0$, and $C = 20$. In one of them $\beta = 0.2$, and in the other, $\beta = 20$. The number of oscillators is $N = 4$. The starting guess uses a suggestion of Watanabe and Swift [26]; it simply uses $h(t)$, the periodic solution of the uncoupled Josephson junction, in place of $g(t)$ and shifts it by 0, $T/4$, $T/2$, and $3T/4$ to get the starting guesses for ϕ_1, ϕ_2, ϕ_3, and ϕ_4. The starting guess takes Q to be C times the average of $\dot{h}(t)$ over one period and $\dot{Q}$ to be zero.

The computation for $\beta = 0.2$ follows the algorithm in section 2 with one small modification. The $\phi_i(\tau)$ are not exactly 2π periodic but increase by 2π as τ increases from 0 to 2π. We represent $\phi_i(\tau) - \tau$ and $\dot{\phi}_i(\tau)$, $1 \le i \le 4$, using Fourier series as

Table 3 *The correct digits of ω are underlined. The algorithm in section 2 is implemented with modifications described in the text. The width of the Fourier series used was 64. The residual error is merely the maximum component of $r(\tau)$, defined in section 2, over $0 \leq \tau < 2\pi$.*

$\beta = 0.2$			$\beta = 20$		
Iteration	ω	Residual error	Iteration	ω	Residual error
0	2.33004377543409	3.0e-3	0	2.34132762154759	6.8 e-1
1	2.33000570267381	5.3e-8	1	2.50011544616387	4.8e-2
2	2.33000570299029	9.4e-14	2	2.49992020054629	3.8e-6
3	2.33000570299029	1.2e-14	3	2.49992002719170	2.7e-13
4	2.33000570299029	1.4e-14	4	2.49992002719170	3.9e-14

2π periodic functions. The width of the Fourier series used was 64. The computed values of the 10 eigenvalues of the monodromy matrix are

```
1.14972325197525 + 5.356810539765e-02i,
1.14972325197525 - 5.356810539765e-02i,
1.00300906019521,
0.999999999999998,
0.882622153149967,
-1.17233411754789e-3 + 4.4552134973842e-04i,
-1.17233411754789e-3 - 4.4552134973842e-04i,
1.39002192156418e-6,
1.21256461043241e-6 + 5.700237506520e-8i,
1.21256461043241e-6 - 5.700237506520e-8i.
```

Watanabe and Swift [26] used multiple scale perturbation analysis and approximated the absolute value of the top two eigenvalues above using formulas that evaluate to 1.12511278376262. The actual absolute value is 1.15097050268390. Their formulas give 1.00224333725148 as the approximation for the third eigenvalue from the top. The eigenvalues above are in close agreement with the numbers in [10]. The fourth eigenvalue is pretty close to 1, its exact value.

The method used for $\beta = 0.2$ fails completely when $\beta = 20$. When $\beta = 20$ the monodromy has multiple eigenvalues very close to 1. As a result, σ_2 in Theorem 3.1 will be very close to zero. However, a simple modification allows us to get around this. Instead of treating the functions ϕ_i and $\dot{\phi}_i$ as different functions for $i = 1, 2, 3, 4$ during every iteration, we pretend that there is only the set ϕ_1 and $\dot{\phi}_1$, and we force the other ϕ_i and $\dot{\phi}_i$ to be copies of this set shifted by a suitable fraction of the period at the end of every iteration. The algorithm then converges quadratically. The eigenvalues of the monodromy are

```
1.00000000000000 + 0.00000000000000i,
0.99999999956928 + 0.00000000000000i,
0.99994524677903 + 0.00000220190766i,
0.99994524677903 - 0.00000220190766i,
0.88195612146459 + 0.00000196311346i,
0.88195612146459 - 0.00000196311346i,
0.88190783340108 - 0.00000000000000i,
0.93882448496301 - 0.00000000000000i,
0.59095372790138 + 0.76821107119497i,
0.59095372790138 - 0.76821107119497i.
```

The formulas in [26] give 0.9999452808964 as the estimate of the absolute value of the third and fourth eigenvalues. The absolute value is actually 0.99994524678145. The Watanabe–Swift estimate for the second eigenvalue is 0.99999999956940. Evidently their perturbative analysis is trustworthy. For $\beta = 0.2$ the splay-phase solution is a saddle and for $\beta = 20$ the splay-phase solution is very weakly attracting.

4.3. A Planar Vector Field with Multiple Limit Cycles. The four-parameter family of planar vector fields

$$\begin{aligned} \dot{x} &= y, \\ \dot{y} &= -(x^3 + rx^2 + nx + m) + (b - x^2)y \end{aligned} \tag{4.1}$$

has been investigated by Dangelmayr and Guckenheimer [2]. When $r = m = 0$, the vector field becomes a normal form for codimension-2 bifurcations with a certain type of symmetry. Dangelmayr and Guckenheimer analyzed this four-parameter family to understand the effect of loss of symmetry. They scaled variables and rewrote the vector field above as a small perturbation of a one-degree-of-freedom Hamiltonian vector field. The Hamiltonian part has exact solutions that are mostly periodic orbits expressible, unsurprisingly, in terms of elliptic integrals. The perturbative analysis has many points of difficulty, but among other things, leads to a region of parameter space with four limit cycles. The parameters $r = 0.87$, $m = -1$, $n = -1.127921667$, and $b = 0.897258546$, used here and in [10], are based on Malo's work [17]. The four limit cycles are shown in Figure 2. Note how close the three inner cycles are to one another. The outermost cycle is attracting and the inner three are, respectively, repelling, attracting, and repelling. For the three inner cycles, the dynamics is slow when they cross the negative x axis but much faster when they cross the positive x axis.

The outermost cycle can be easily computed using the algorithm in section 2. But the three inner orbits are much harder to compute accurately. Figure 3 helps explain the source of the difficulty. The entries of the fundamental matrix Y of the inner cycles start with values near 1, vary over a range of more than 10^5, and at the end of the cycle, the entries of the monodromy are again of the order 1. This wide variation inevitably leads to a loss of 10 digits of precision in the monodromy. The peculiar behavior of $Y(\tau)$ is concentrated in a small part of the period, and to capture it correctly the ODE solver used in step 4 of the algorithm has to be very accurate.

To find the four periodic orbits accurately, we modified the algorithm in section 2. All along the x axis, the vector field is directed in the orthogonal y direction. Therefore, the negative x axis is a natural choice for a Poincaré section. The modified algorithm starts at a point x_0 on this section and follows the trajectory from that point accurately until it cuts the section again at x_0' in the same direction as the vector field at x_0. We used an eighth-order Runge–Kutta method due to Fehlberg [11] and a stepsize of 0.005. The fundamental matrix of the linearization along the trajectory is also computed. Assume that the fundamental matrix at x_0' is M. It will be close to the monodromy of the cycle if the initial point x_0 is close to being on the orbit. Instead of following the trajectory again from x_0', we use the principles of section 2 and solve the 2×2 linear system

$$(I - M)\delta x = x_0' - x_0$$

for δx and take $x_1 = x_0 + \delta x$ as the starting point for a new iteration.

The trajectories were followed forward in time for attracting orbits and backward in time for repelling orbits. The starting values of x_0 were -1.3, -0.9736, -0.9712,

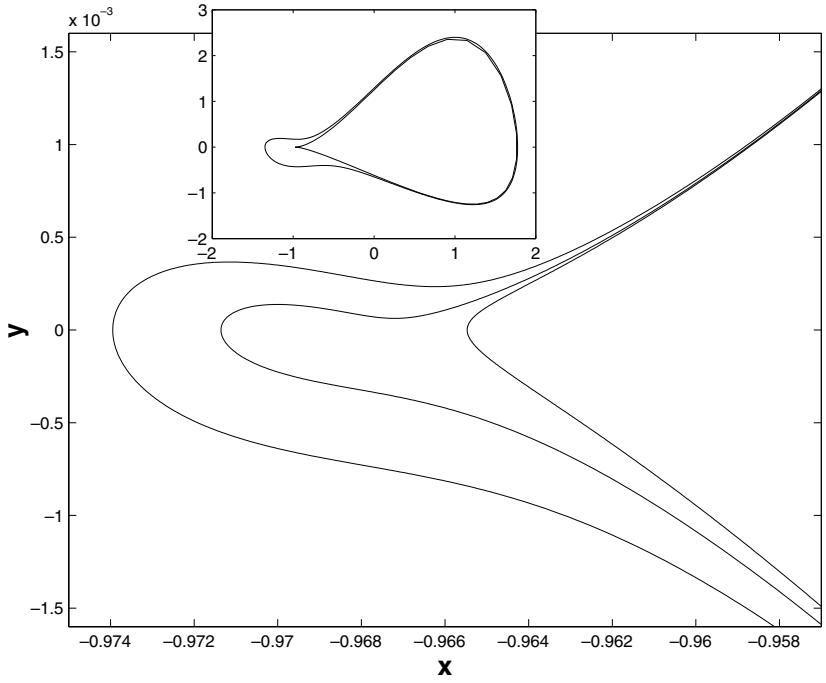

Fig. 2 *Four limit cycles of* (4.1). *The parameters r, m, n, and b take values given in the text. The inset shows all four cycles, but the three inner cycles are indistinguishable and appear as one curve. The outer plot shows a portion of the three inner cycles around the narrow turn.*

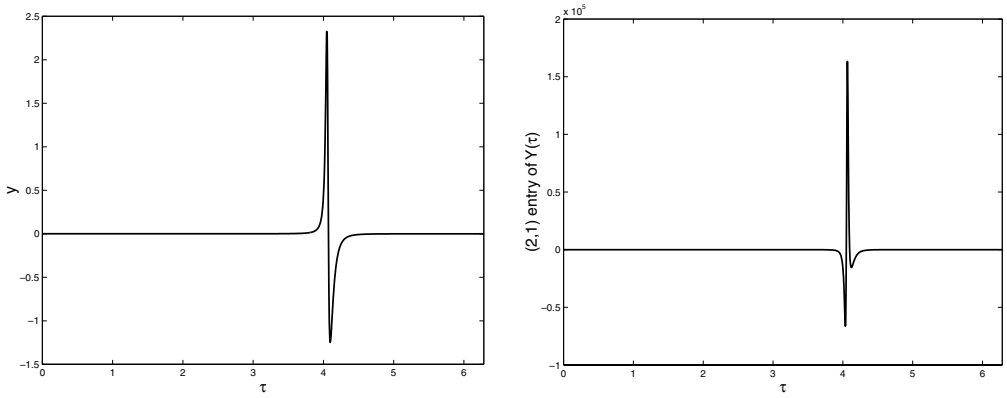

Fig. 3 *The two plots show $y(\tau)$ vs. τ and the first entry of the second row of $Y(\tau)$ vs. τ for the middle of the three inner orbits. The sharp rise and fall of y implies that a Fourier representation of y will need a lot of coefficients.*

and -0.9654 for the orbits from outermost to innermost. Since a loss of 10 digits is inevitable for the three inner orbits, we used floating point arithmetic with 128 bits of precision. The eighth-order Runge–Kutta method, which does most of the trajectory following, was implemented using the GNU MP package [7]. Only a small part of the trajectory was followed in MATLAB. Table 4 shows that the convergence is quadratic.

Table 4 *The $x(0)$ column gives the starting position on the negative x axis for each iteration. The top eigenvalue of M is 1 for the exact orbit. The correct digits of the period T are underlined. The convergence is clearly quadratic.*

Iteration	$T = 2\pi/\omega$	$x(0)$	Top eigenvalue of M
0	1.555318923187230e2	−0.97120000000000	1.08267992336501
1	1.510992886709926e2	−0.97135250141984	1.00307045291158
2	1.509158025428224e2	−0.97135911618029	1.00000629224100
3	1.509154245688264e2	−0.97135912983162	1.00000000002695
4	1.509154245672065e2	−0.97135912983168	0.99999999999999

Table 5 *Data for the four periodic orbits from outermost to innermost. The $x(0)$ column gives the point of intersection with the negative x axis.*

Periodic orbit	$T = 2\pi/\omega$	$x(0)$	Characteristic multiplier
1	11.43951544634134	−1.34900179268526	0.49598496726985
2	103.8895372178061	−0.97394763366240	1.62267497161985
3	150.9154245672065	−0.97135912983168	0.29226469348440
4	79.14808431110376	−0.96547045585340	6.33296668940165

Table 5 gives the periods and the characteristic multipliers of all four periodic orbits with 15 digits of precision. The periods of the three inner orbits are very different even though they stick together closely. Most of the difference in period comes from the slow turn around the x axis.

If the value of b is increased or decreased for fixed n, r, and m, two of the periodic orbits fuse together in a saddle node bifurcation. If n is changed slightly, then again there are two values of b where saddle node bifurcations occur. Thus for $r = 0.87$ and $m = -1$, there are two saddle node bifurcation curves in the $n - b$ plane. In fact, according to comments in [10], the two curves intersect at a cusp where presumably all the four periodic orbits are fused together. Finding 15 digits of the parameter values at the cusp and the periodic orbit at those parameter values could be an interesting problem. It does not appear completely trivial to construct a cubic vector field in the plane which has four limit cycles like the one above. Hilbert's 16th problem asks for the maximum possible number of limit cycles for a planar vector field of any given degree. Dangelmayr and Guckenheimer [2] did not comment on Hilbert's 16th problem but Guckenheimer's suggestions in [9] have much in common with the analysis in [2].

4.4. Hill's Problem. In 1878, Hill [13] derived the following equations to describe the motion of the moon around the earth:

$$\ddot{x} - 2\dot{y} = \frac{\partial \Omega}{\partial x},$$
$$\ddot{y} + 2\dot{x} = \frac{\partial \Omega}{\partial y}.$$

Here, $\Omega = 3x^2/2 + (x^2 + y^2)^{-1/2}$. The Jacobi integral $2\Omega - \dot{x}^2 - \dot{y}^2$ is constant along the solutions of Hill's equation. In fact, it has been proven that it is the only constant expressible algebraically. With proper choice of units, Hill's equation describes the motion of the moon around the earth in a coordinate system that rotates with the sun. The motion of the moon is assumed to be planar, which it is nearly, and the perturbing effect of the sun is taken into account up to first order. Hill's equation

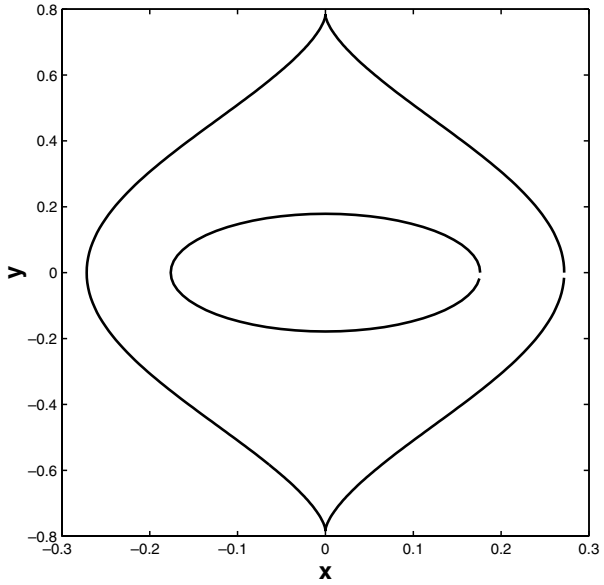

Fig. 4 *Two periodic orbits of Hill's equation. The inner orbit is a good approximation to the lunar orbit. The outer orbit is called the orbit of maximum lunation. Both $\dot{x}$ and $\dot{y}$ are zero at the intersection of the orbit of maximum lunation with the y axis.*

can be derived from the restricted three-body problem using a scaling argument, a derivation whose "simplicity and directness is a source of true joy" [21]. Szebehely's classic work on the three-body problem [21] discussed Hill's equation. Lunar theories based on Hill's work are discussed in many sources on celestial mechanics, including [20].

Figure 4 shows two periodic orbits of Hill's equation. The inner orbit has $1/\omega = 0.08084893380831 = \frac{n_m}{n_s - n_m}$, where $n_s = 365.256371$ and $n_m = 27.321661$. This special value of the period makes the inner orbit an excellent approximation for the moon's orbit around the earth. Between the inner and outer orbits, there is a family of periodic orbits. If the moon were following the outer orbit, called the orbit of maximum lunation, it would come to a complete halt at the y axis (in the rotating coordinate system) before starting off again, pulled by the earth and by the sun. Hill's research on lunar theories achieved quick recognition and are influential even today. Speaking of Hill's work and progress in celestial mechanics, Poincaré said in the preface to his *New Methods of Celestial Mechanics* [22], "In this work, unfortunately incomplete, we are permitted to perceive the germ of the major part of progress which science has since made." In what sense does Poincaré regard the work as incomplete? Perhaps he was referring to the Hill–Brown lunar theory later developed by Brown based on Hill's work; or he might have been bothered by the absence of rigor in some of Hill's calculations.

Table 6 gives the data for the two orbits. This is possibly the most accurate determination of the two orbits done so far. Both the orbits are symmetric with respect to both the x and the y axes. Thus $y(T/4)$ will give the intersection of the periodic orbit with the y axis. Further, $y(0) = 0$, $\dot{x}(0) = 0$, and $\dot{y}(T/4) = 0$ for both the orbits. The monodromy, in both cases, has 1 as a double eigenvalue. But the

Table 6 *Data for the inner and outer orbits in Figure* 4. *The* λ_i *are the eigenvalues of the monodromy. The last two numbers in the second column must be read together. This table reports* $1/\omega$ *instead of* ω *or the period* $T = 2\pi/\omega$ *to facilitate comparison with Table* II *in Chapter* 10 *of* [21]. *The latter table gives data accurate to five digits but does not give the eigenvalues of the monodromy. Only five of the seven digits of* $1/\omega$ *of the orbit of maximum lunation reported in that table are accurate.*

	Lunar orbit	Orbit of maximum lunation
$1/\omega$	0.08084893380831	0.56095735370278
Jacobi constant	6.50887947496948	2.55790629858017
$x(0)$	0.17609701771836	0.27179733000554
$y(T/4)$	0.17864404564174	0.78188946995836
λ_i	1.00000153080612	454.161613940992
	0.99999846919563	1.00000484977549
	0.90054668719805	0.99999515023284
	± 0.43475931753079i	0.00220185935677

eigenvalues in Table 6 approximate 1 very poorly. It is possible to prove that 1 is a double eigenvalue of the monodromy with a nontrivial Jordan block in both cases. Consequently, even though the monodromy is accurate, these two eigenvalues are not very accurate.

To approximate the lunar orbit, we generated a starting approximation using MATLAB's `ode45` and Table II in Chapter 10 of [21]. Step 5 of the algorithm in section 2 tries to compute a correction to x, y, $\dot{x}$, and $\dot{y}$ at $t = 0$, and to $\delta\omega$. However, since 1 is a double eigenvalue of M, the linear system of dimension 5 in step 5 will be singular or nearly singular. To compute the correction to these quantities, we set $\delta\omega = 0$, since what we seek is a lunar orbit of known period and $\delta y = 0$ so that $y(0) = 0$ across iterations. This leads to a least squares problem of size 5×3 to obtain corrections to x, $\dot{x}$, and $\dot{y}$. We used a Fourier series of width 64 and filtered out 20% of the frequencies at the high end after each iteration. The errors in successive approximations, measured using the Jacobi constant, were $1.3\mathrm{e}-5$, $1.4\mathrm{e}-8$, $6.2\mathrm{e}-15$, and $4.4\mathrm{e}-15$.

The orbit of maximum lunation is harder to get. That orbit is defined by the condition $\dot{x} = \dot{y} = 0$ after one quarter-period when the orbit is at the y axis. There is exactly one periodic orbit that crosses the x axis at any given point in the vicinity of the orbit of maximum lunation. All these orbits are symmetric about the x and the y axes. Therefore, $\dot{y}(T/4)$, which is $\dot{y}$ at one quarter-period, is zero for all these orbits. To solve for the orbit of maximum lunation, we need to find $x(0)$ such that the periodic orbit passing through $x = x(0)$ and $y = 0$ at $t = 0$ has $\dot{x}(T/4) = 0$ in addition to $\dot{y}(T/4) = 0$. Starting data from [21] was used to construct a periodic orbit very near (error $\approx 1\mathrm{e}-5$) the orbit of maximum lunation. We varied $x(0)$, keeping $y(0) = 0$. Every time $x(0)$ was varied, a new periodic orbit had to be constructed. This time we solved a 5×3 least squares problem in step 5 of the algorithm to obtain corrections to $\delta\omega$, $\dot{x}(0)$, and $\dot{y}(0)$, while keeping $x(0)$ and $y(0) = 0$ fixed. Finally, we applied the secant method [3], which can be used to find the zero of a smooth function of one real variable. Two steps of the secant method were needed to solve for an $x(0)$ such that $\dot{x}(T/4) = 0$. The final solution to the orbit of maximum lunation has an error of about $1\mathrm{e}-15$. The error is measured using the Jacobi integral *and* $\dot{x}$ at one quarter-period.

In finding the orbit of maximum lunation, we used Fourier series of width 512 and filtered out 40% of the frequencies at the high end after each iteration. It is

feasible to use Fourier series of width n for large n because the cost of each iteration is proportional to $n \log n$. In the direct implementation used here, the cost is proportional to $n^2 \log n$, but see [25]. As we noted in section 1, the cost of each iteration is proportional to n^3 for harmonic balance methods, which makes use of Fourier series of large width prohibitively expensive.

The three inner limit cycles in the planar vector field of the previous example combine slow and rapid variation. The adaptivity of AUTO [6] and the Guckenheimer–Meloon algorithms [10] may make them more suitable for such examples. However, conditioning implies that the three limit cycles cannot be computed with accuracy greater then `1e-5` in IEEE arithmetic no matter what algorithm is used. Extended precision has to be used to compute the limit cycles accurately. We have derived a multiple shooting version of the Lindstedt–Poincaré algorithm [25]. Multiple shooting was not needed for any of the examples in this paper. Multiple shooting could be of use for computing a periodic orbit only if its computation is severely ill-conditioned, with condition number greater than `1e+10`.

5. Conclusion. This paper has concentrated exclusively on the computation of periodic orbits. Computing periodic orbits is a basic step in computing bifurcations of several kinds. We hope the algorithms given in sections 2 and 4.3 can be made the basis for computing bifurcations. The Lindstedt–Poincaré technique has been applied to partial differential equations [14]. The algorithm in section 2 may also be applicable to partial differential equations.

Acknowledgment. I thank Prof. John Guckenheimer for drawing my attention to the literature on harmonic balancing.

REFERENCES

[1] W.G. Choe and J. Guckenheimer, *Computing periodic orbits with high accuracy*, Comput. Meth. Appl. Mech. Engrg., 170 (1999), pp. 331–341.
[2] G. Dangelmayr and J. Guckenheimer, *On a four parameter family of planar vector fields*, Arch. Rational Mech. Anal., 97 (1987), pp. 321–352.
[3] J.E. Dennis, Jr. and R.B. Schnabel, *Numerical Methods for Unconstrained Optimization and Nonlinear Equations*, SIAM, Philadelphia, 1996.
[4] E.J. Doedel, *Finite difference collocation methods for nonlinear two-point boundary value problems*, SIAM J. Numer. Anal., 16 (1979), pp. 173–185.
[5] E.J. Doedel, *Nonlinear numerics*, J. Franklin Inst. B, 334 (1997), pp. 1049–1073.
[6] E.J. Doedel, A.R. Champneys, T.F. Fairgrieve, Y.A. Kuznetsov, B. Sandstede, and X. Wang, *AUTO* 97: *Continuation and Bifurcation Software for Ordinary Differential Equations*, available at ftp.cs.concordia.ca/pub/doedel/auto (156 pages), 1998.
[7] T. Granlund, *GNU MP*, Free Software Foundation, Boston, 1996, available at www.gnu.org.
[8] A. Griewank, D. Juedes, and J. Utke, *ADOL-C: A package for automatic differentiation of algorithms written in C/C++*, ACM Trans. Math. Software, 22 (1996), pp. 131–167.
[9] J. Guckenheimer, *Computer proofs for bifurcations of planar dynamical systems*, in Computational Differentiation: Techniques, Applications, and Tools, SIAM, Philadelphia, 1996, pp. 229–237.
[10] J. Guckenheimer and B. Meloon, *Computing periodic orbits and their bifurcations with automatic differentiation*, SIAM J. Sci. Comput., 22 (2000), pp. 951–985.
[11] E. Hairer, S. Norsett, and G. Wanner, *Solving Ordinary Differential Equations* I, 2nd rev. ed., Springer-Verlag, New York, 1993.
[12] J. Hale, *Ordinary Differential Equations*, 2nd ed., Krieger, Malabar, FL, 1988.
[13] G. Hill, *Researches in lunar theory*, American Journal of Mathematics, 1 (1878), pp. 129–245.
[14] J. Kevorkian and J.D. Cole, *Multiple Scale and Singular Perturbation Methods*, Springer-Verlag, New York, 1996.

[15] S.L. Lau, Y.K. Cheung, and S.Y. Wu, *A variable parameter incrementation method for dynamic instability of linear and nonlinear elastic systems*, J. Appl. Mech., 49 (1982), pp. 849–853.
[16] F.H. Ling and X.X. Wu, *Fast Galerkin methods and its application to determine periodic solutions of non-linear oscillators*, Int. J. Non-Linear Mech., 22 (1987), pp. 89–98
[17] S. Malo, *Rigorous Computer Verification of Planar Vector Field Structure*, Ph.D. Thesis, Cornell University, Ithaca, NY, 1993.
[18] A.H. Nayfeh, *Introduction to Perturbation Techniques*, Wiley, New York, 1993.
[19] C. Robinson, *Dynamical Systems: Stability, Symbolic Dynamics, and Chaos*, CRC Press, Boca Raton, FL, 1999.
[20] W.M. Smart, *Celestial Mechanics*, Wiley, London, 1953.
[21] V. Szebehely, *Theory of Orbits*, Academic Press, New York, 1967.
[22] H. Poincaré, *New Methods of Celestial Mechanics*, D. Goroff, ed., American Institute of Physics, New York, 1993.
[23] L.N. Trefethen, *Spectral Methods in MATLAB*, SIAM, Philadelphia, 2000.
[24] D. Viswanath, *Global errors of numerical ODE solvers and Lyapunov's theory of stability*, IMA J. Numer. Anal., 21 (2001), pp. 387–406.
[25] D. Viswanath, *A faster algorithm for computing periodic orbits*, in preparation.
[26] S. Watanabe and J. Swift, *Stability of periodic solutions with series arrays of Josephson junctions with internal capacitance*, J. Nonlinear Sci., 7 (1997), pp. 503–536.